

**Temperature and thickness evolution and epitaxial breakdown in highly strained BiFeO<sub>3</sub> thin films**Anoop R. Damodaran,<sup>1</sup> Sungki Lee,<sup>1</sup> J. Karthik,<sup>1</sup> Scott MacLaren,<sup>2</sup> and Lane W. Martin<sup>1,\*</sup><sup>1</sup>*Department of Materials Science and Engineering and Materials Research Laboratory, University of Illinois, Urbana-Champaign, Urbana, Illinois 61801, USA*<sup>2</sup>*Center for Microanalysis of Materials, Materials Research Laboratory, University of Illinois, Urbana-Champaign, Urbana, Illinois 61801, USA*

(Received 17 October 2011; published 13 January 2012)

We present the temperature- and thickness-dependent structural and morphological evolution of strain-induced transformations in highly strained epitaxial BiFeO<sub>3</sub> films deposited on LaAlO<sub>3</sub> (001) substrates. Using high-resolution x-ray diffraction and temperature-dependent scanning-probe-based studies, we observe a complex temperature- and thickness-dependent evolution of phases in this system. A thickness-dependent transformation from a single, monoclinically distorted, tetragonal-like phase to a complex mixed-phase structure in films with thicknesses up to  $\sim 200$  nm is the consequence of a strain-induced spinodal instability in the BiFeO<sub>3</sub>/LaAlO<sub>3</sub> system. Additionally, a breakdown of this strain-stabilized metastable mixed-phase structure to nonepitaxial microcrystallites of the parent rhombohedral structure of BiFeO<sub>3</sub> is observed to occur at a critical thickness of  $\sim 300$  nm. We further propose a mechanism for this abrupt breakdown that provides insight into the competing nature of the phases in this system.

DOI: [10.1103/PhysRevB.85.024113](https://doi.org/10.1103/PhysRevB.85.024113)

PACS number(s): 77.80.-e, 77.84.Bw, 81.15.Np

**I. INTRODUCTION**

BiFeO<sub>3</sub> is a room-temperature multiferroic perovskite exhibiting antiferromagnetism that is coupled with ferroelectric order.<sup>1,2</sup> At room temperature, bulk BiFeO<sub>3</sub> assumes a rhombohedrally distorted perovskite structure with an *R3c* space group.<sup>3</sup> Only recently have researchers begun in earnest to analyze the structure of new polymorphs observed in highly strained BiFeO<sub>3</sub> films. Early theoretical<sup>4,5</sup> and experimental<sup>6-8</sup> studies suggested the possibility of a tetragonally distorted phase (derived from a structure with *P4mm* symmetry, *a*  $\sim 3.665$  Å, and *c*  $\sim 4.655$  Å) with a large spontaneous polarization. Soon after, enhanced electromechanical strains as large as 4–5% were demonstrated in so-called mixed-phase BiFeO<sub>3</sub> thin films that exhibit a strain-induced structural mixture in which several polymorphs coexist.<sup>8</sup> The enhanced electromechanical response in these materials has been attributed to the thickness-dependent development of this complex mixed-phase structure and the ability of this material to reversibly transform under applied electric fields between these various phases.<sup>9,10</sup> Since these studies, additional information has come forth about these highly strained films, including the observations that the so-called tetragonal-like phase is monoclinically distorted<sup>11-14</sup> and that other intermediate phases are present and play an essential role in the mixed-phase structures.<sup>9</sup> Recent reports of structural, magnetic, and ferroelectric transformations<sup>15-17</sup> near room temperature in these materials suggest promise for giant piezoelectric, magnetoelectric, and piezomagnetic responses.

Further insight into the nature of the thickness-dependent evolution of these highly strained BiFeO<sub>3</sub> films can be gained by investigating related work on the epitaxial growth of other metastable phases.<sup>18</sup> It has long been known that epitaxial thin-film strain has a large role to play in the evolution of thin-film structure. Typically in a mismatched film-substrate scenario, the film is coherently strained (referred to as a commensurate state) to some point where it becomes too

energetically costly to continue to accommodate all of the strain in the film. At this point, so-called discommensuration (or the formation of strain-relieving defects) occurs, driving the system into an incommensurate state. The mean separation distance between these strain-relieving defects generally decreases as the mismatch increases. Often these defects are misfit dislocations that form ordered arrays at the substrate-film interface.<sup>19,20</sup> The density of these misfit dislocations will increase as the film thickness is increased until the total strain in the film is reduced to zero and the lattice parameters return to those of the bulk. Following the nomenclature used by Bruinsma and Zangwill,<sup>18</sup> we will refer to coherent-incoherent transitions resulting from a variation in thickness (*h*) and commensurate-incommensurate transitions resulting from variations in lattice misfit (*f*).

It has been observed that in metal systems, where dislocation motion is relatively easy, predicted values of critical thicknesses (*h<sub>c</sub>*) and the thickness dependence of coherency loss follow each other closely.<sup>21</sup> Oxide-based systems, however, are widely observed to deviate from these predictions due to large kinetic barriers to dislocation nucleation and migration.<sup>22</sup> Thus, in these systems, alternative pathways for strain relaxation are possible—including having the film adopt a crystal structure that is well lattice matched to the substrate, but that is different from the bulk structure of the film material. This process has been referred to as *pseudomorphism* and the pseudomorphic phase is often coherently strained to the substrate. We note that pseudomorph may be a misnomer and that polymorph may be the more accurate term here. Pseudomorphism, which literally means false form, comes from mineralogy and refers to a compound or mineral that has taken on the shape or structure of another mineral. In general this can be mechanical, structural, or chemical in nature. Polymorphism, on the other hand, refers to the ability of a solid material (with a single chemical composition) to exist in more than one form or crystal structure. The study of such polymorphs dates back to the 1950s when alkali halide films

were observed to undergo a so-called pseudomorphic phase transformation.<sup>23</sup> Additionally, early molecular-beam epitaxy studies found that in certain metal systems, polymorphic phase transitions are possible. For instance, work on Sb (which normally possesses a tetragonal bcc structure (white tin) with  $a = 5.831 \text{ \AA}$  and  $c = 3.181 \text{ \AA}$  at room temperature) found that this material adopted a low-temperature diamond structure (grey tin,  $a = 6.489 \text{ \AA}$ ) when deposited on (001) InSb and CdTe ( $a = 6.48 \text{ \AA}$ ).<sup>24</sup> By undergoing the polymorphic transformation, the Sb avoids an unfavorable lattice mismatch and strain condition. Likewise, similar results have been obtained for Co films on GaAs.<sup>25</sup> More surprising in this case, films of Co less than 100 nm in thickness were found to grow as a previously unknown, metastable bcc version ( $a = 2.819 \text{ \AA}$ ) on GaAs (110), while films greater than 100 nm were found to transform to the bulk hcp structure. More recently, Bruinsma and Zangwill<sup>18</sup> proposed a thickness-dependent structural phase diagram as a function of the geometric misfit between the substrate and film and overall film thickness to help explain such effects. These predictions also included an intermediate strain regime where the film evolves from a single-phase, highly strained, metastable structure to a spinodal-modulated, mixed-phase structure before eventual breakdown to micro-

crystallites of the bulk stable phase. In the remainder of the paper, we will investigate the applicability of this model to the observed features of the thickness-dependent growth of highly strained BiFeO<sub>3</sub> films on LaAlO<sub>3</sub> (001) substrates. We will establish a thorough understanding of the growth, thickness- and temperature-dependent evolution, phase stability, and the role and influence of the parent rhombohedral phase on these highly strained structures. The current work examines the evolution of these various phases, provides a proposed mechanism for the evolution of the mixed-phase structures important for the large electromechanical responses, examines the eventual epitaxial breakdown of this system, and frames these results as a competition between the thermodynamically stable equilibrium rhombohedral phase and the strain-induced polymorphs.

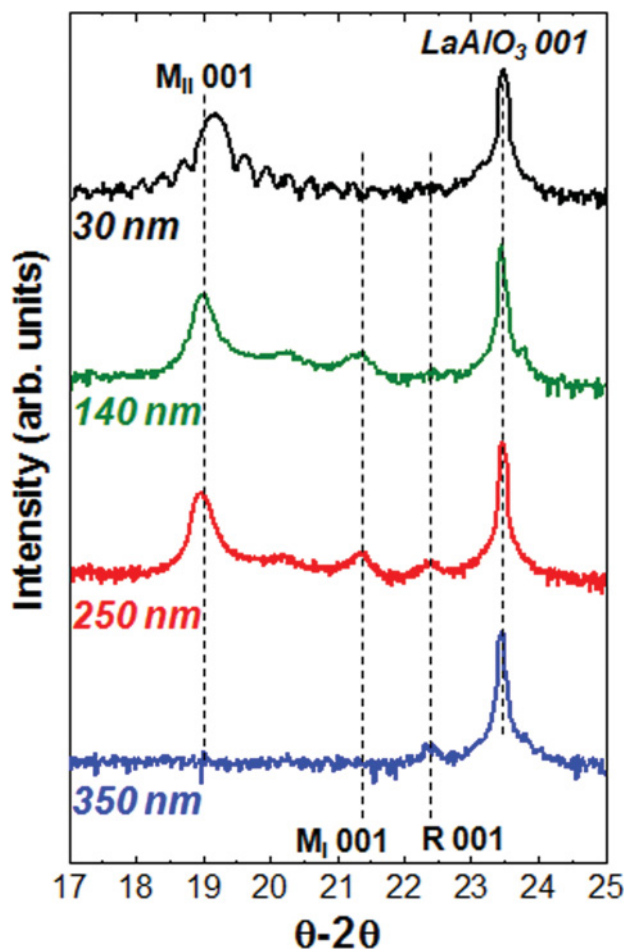


FIG. 1. (Color online) X-ray diffraction about the 001-diffraction condition of BiFeO<sub>3</sub>/LaAlO<sub>3</sub> (001) heterostructures for films of (top to bottom) 30 nm, 140 nm, 250 nm, and 350 nm thickness.

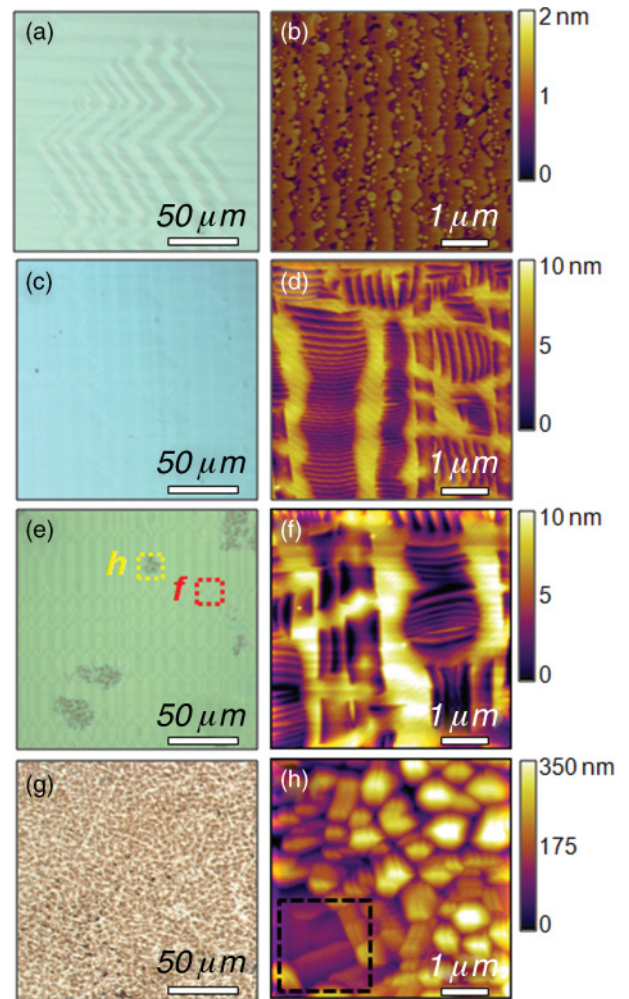


FIG. 2. (Color online) Optical (left) and atomic-force microscopy (right) images of BiFeO<sub>3</sub>/LaAlO<sub>3</sub> (001) heterostructures of various thicknesses. (a) and (b) are images for a 30-nm-thick film and (c) and (d) show a 140-nm-thick film. (e) Reveals the formation of different types of structures in 250-nm-thick films. Close inspection of (f) the smooth areas reveals results consistent with thinner films and investigations (h) of rough regions reveal rough microstructures. (g) An optical micrograph of a 350-nm-thick film, which is found to possess only the rough microstructure.

## II. EXPERIMENT

Epitaxial BiFeO<sub>3</sub> films of thickness 20–400 nm were synthesized via pulsed-laser deposition from Bi<sub>1.1</sub>FeO<sub>x</sub> targets at 700 °C in oxygen pressures of 100 mTorr on single-crystal LaAlO<sub>3</sub> (001) substrates and were cooled in oxygen pressures of 760 Torr. The laser fluence and repetition rate were maintained at 1.45 J/cm<sup>2</sup> and 10 Hz, respectively, for all growths resulting in an effective growth rate of 0.28 Å/s. Care was taken to assure uniform deposition and appropriate chemistry and thus no single target was used to deposit more than 75 nm of material. Detailed structural information for the various films was obtained using high-resolution x-ray diffraction (XPert MRD Pro equipped with a PIXcel detector, Panalytical) including  $\theta$ - $2\theta$  scans and reciprocal space maps (RSMs). Topographic studies of the as-grown films were carried out using temperature-dependent (25–300 °C) atomic-force microscopy (AFM) (Cypher and MFP-3D, Asylum Research). The surface structure and cross sections of the as-grown films were also observed using a Hitachi S-4800 high-resolution scanning electron microscope (SEM).

## III. RESULTS AND DISCUSSIONS

Typical  $\theta$ - $2\theta$  x-ray diffraction studies about the 001-diffraction condition of BiFeO<sub>3</sub> films of thicknesses 30, 140, 250, and 350 nm (Fig. 1) reveal an interesting evolution in the structure with thickness. Following the nomenclature established in recent studies,<sup>9</sup> the various phases observed are labeled as the rhombohedral parent phase (R phase,  $c = 3.96$  Å), the intermediate monoclinic phase (M<sub>I</sub> phase,  $c = 4.17$  Å), and the monoclinically distorted, tetragonal-like phase (M<sub>II</sub> phase,  $c = 4.67$  Å). The 30-nm-thick film exhibits a single peak corresponding to an out-of-plane lattice parameter  $c$  of  $\sim 4.63$  Å, consistent with the M<sub>II</sub> phase. Upon increasing the film thickness, additional peaks corresponding first to the M<sub>I</sub> phase and subsequently to the bulk-like R phase begin to appear. From our studies, we have observed that in films of

thickness less than  $\sim 200$  nm, the peak corresponding to the R phase has very low intensity, or is totally absent in some cases. By the time the thickness reaches  $\sim 250$  nm, the presence of an R-phase peak is more noticeable for most films, and by a thickness of  $\sim 350$  nm, only the peak corresponding to the R phase is observed and all other peaks are completely absent. It should also be noted that the R-phase peak is considerably less intense than the peaks for the M<sub>II</sub> phase in the thinner films and, in general, shows lower diffraction intensities throughout the films studied. We also note that the out-of-plane lattice parameter of the M<sub>II</sub> phase increases from 4.63 to 4.68 Å as we transition from the 30- to 250-nm-thick films (Fig. 1). This suggests a rather complex thickness-dependent evolution and strain-relaxation process in these films.

Such observations present two important questions: what happens to the M<sub>II</sub> phase in thicker films and why does the R-phase peak intensity remain so low even in thick films? Here we develop a detailed picture of the complex behavior observed in these diffraction experiments and provide insight into the thickness-dependent evolution of this complex system. An understanding of the structural evolution is obtained by investigation of the surface topography of these films at various magnifications using both optical microscopy and AFM (Fig. 2). Under the optical microscope, the 30-nm-thick films are found to have an optically smooth surface (note the presence of the structural twins in the LaAlO<sub>3</sub> substrate visible in the image) [Fig. 2(a)], which is consistent with the AFM images [Fig. 2(b)] that exhibit only the M<sub>II</sub> phase with atomically smooth terraces, separated by single unit-cell step heights ( $\sim 4.65$  Å). Likewise, the optical micrographs of the 140-nm-thick films reveal these films to be optically smooth [Fig. 2(c)], and upon close inspection using AFM, we observe mixed-phase topography consisting of regions of atomically flat terraces of the M<sub>II</sub> phase [bright areas, Fig. 2(d)] and mixed-phase regions consisting of an intimate mixture of the M<sub>I</sub> and M<sub>II,tilt</sub> phases [striped regions, Fig. 2(d)], consistent with previous reports.<sup>9</sup> Such mixed-phase regions, which are essential for the large electromechanical responses observed

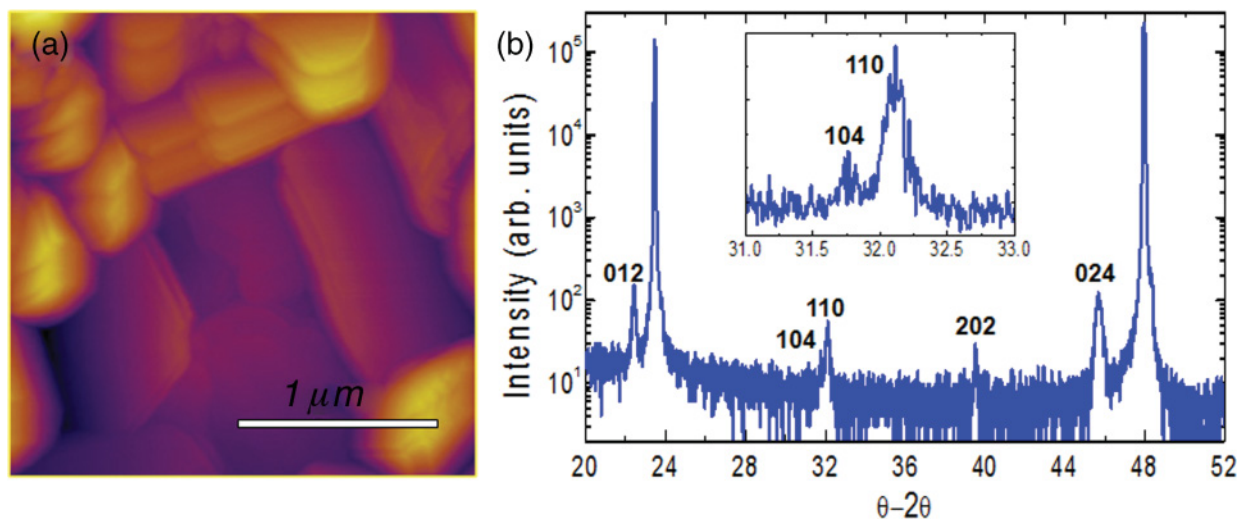


FIG. 3. (Color online) (a) High-resolution atomic-force microscopy image of micron-sized crystallites found in films  $>250$  nm thick. (b) X-ray diffraction pattern of a 350-nm-thick BiFeO<sub>3</sub>/LaAlO<sub>3</sub> (001) heterostructure reveals signatures of the parent rhombohedral phase.

in these materials, consist of an intimate mixture of highly distorted phases, including the intermediate  $M_I$  phase (which is tilted nearly  $2.8^\circ$  from the sample normal) and the so-called  $M_{II, \text{tilt}}$  phase (which has the same  $c \sim 4.67 \text{ \AA}$  as the  $M_{II}$  phase, but is tilted by  $1.6^\circ$  from the sample normal).

An inspection of optical micrographs of the 250-nm-thick films, on the other hand, reveals a surface that is mostly smooth with a number of rough regions [Fig. 2(e)]. We note that the fraction of these rough regions scales with thickness and does not appear to grow with additional time spent at high temperatures without additional material being added to the surface. *Ex situ* anneals at 500–600 °C in oxygen for over 20 hours did not result in a change in the fraction of the rough regions. AFM studies of the optically flat regions [red box in Figs. 2(e) and 2(f)] once again reveal topography consistent with flat plateaus of the  $M_{II}$  phase and striped mixed-phase regions. We note that upon increasing the thickness from 140 to 250 nm, the surface depressions associated with the mixed-phase regions increase greatly from  $\sim 7$  to  $\sim 11$  nm, respectively. Interestingly, however, AFM studies of the same sample in the rough regions [yellow box in Figs. 2(e) and 2(h)] show a significantly roughened surface with a peak-to-valley

height scale of over 200 nm (nearly the entire thickness of the film) without any resemblance to the mixed-phase structures observed elsewhere on this sample. Further inspection of the 350-nm-thick films under the optical microscope reveals that the rough regions have grown dramatically to cover the entire film surface [Fig. 2(g)]. An analysis of these films with AFM revealed surface morphologies similar to that observed in Fig. 2(h). The region within the black box in Fig. 2(h) is consistent with regions observed across this and other samples in this thickness range, and is indicative of the formation of microcrystallites of the parent R phase of  $\text{BiFeO}_3$ .

Figure 3(a) is a high-resolution AFM image of the area highlighted in Fig. 2(h) and reveals that the rough regions possess micron-sized crystallites with well-defined facets. These features bear a resemblance to  $\text{BiFeO}_3$  single crystals,<sup>26–28</sup> which exhibit large flat (012) surfaces (using the crystallographic reference frame of the parent rhombohedral structure). Detailed high-resolution x-ray diffraction scans of our 350 nm samples have allowed us to obtain evidence for a number of peaks corresponding to the bulk-like R phase of  $\text{BiFeO}_3$  [Fig. 3(b)]. These diffraction patterns can be indexed by peaks corresponding to the most intense reflections from

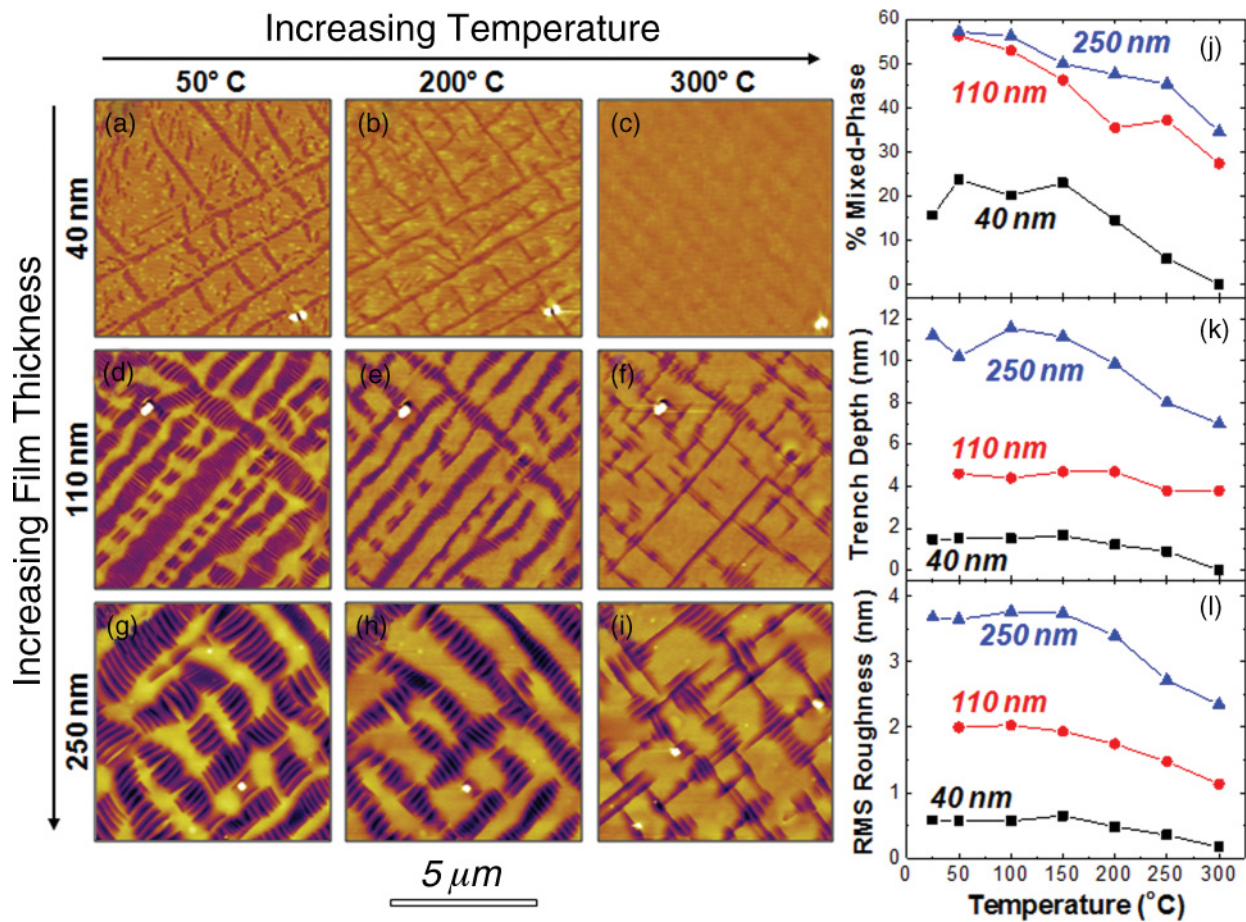


FIG. 4. (Color online) Atomic-force microscopy study of the evolution of surface morphology with increasing temperature from 50 to 300 °C for films with (a)–(c) 40 nm, (d)–(f) 110 nm, and (g)–(i) 250 nm thickness. Corresponding analysis of temperature-dependent evolution of properties, including (j) the relative fraction of the mixed-phase structure at the surface, (k) the average depth of the mixed-phase trenches relative to the surrounding  $M_{II}$  phase, and (l) the root-mean-square (rms) roughness of the samples. Note the general trend to decrease the fraction of the mixed-phase region with increasing temperature, and complete disappearance of the mixed phase in thinner films.

the diffraction patterns of BiFeO<sub>3</sub> single crystals. We have even observed unique features of the bulk R-phase diffraction pattern, such as the splitting of the 104- and 110-diffraction peaks in such films. This combination of x-ray diffraction and AFM strongly suggests that the rough, patchy regions are in fact regions of the bulk-like R phase of BiFeO<sub>3</sub> that grow at the expense of the M<sub>I</sub> and M<sub>II</sub> phases in a nonepitaxial manner. We note that for each thickness reported here, we have included in the same growth a DyScO<sub>3</sub> (110) substrate for further analysis and comparison of the rhombohedral-like thin-film phase. A similar inspection of the codeposited BiFeO<sub>3</sub>/DyScO<sub>3</sub> (110) films reveals smooth surfaces for all films up to and including the 350-nm-thick films, and show no evidence of second phases from x-ray diffraction.

We can further advance our understanding of the mechanism of strain accommodation and epitaxial breakdown in this system by analyzing the change in surface structure of a number of BiFeO<sub>3</sub> films upon heating from room temperature to 300 °C. Figure 4 shows AFM topography images of films of three representative thicknesses, 40 nm [Figs. 4(a)–4(c)], 110 nm [Figs. 4(d)–4(f)], and 250 nm [Figs. 4(g)–4(i)], at three temperatures (from left to right, 50, 200, and 300 °C). At any given temperature, the films reveal an increasing fraction of the mixed-phase regions with increasing film thickness (consistent with prior reports).<sup>8</sup> The reported fraction of the mixed phase is calculated as the areal fraction of the mixed-phase regions relative to the entire area of the sample [Fig. 4(j)]. We also report the depth of the mixed-phase stripe regions relative to the atomically flat plateau regions of the M<sub>II</sub> phase [trench depth, Fig. 4(k)] and the root-mean-square (rms) roughness of these films, which is an indicator of the volume fraction of the mixed-phase regions in these films [Fig. 4(l)].

Beginning with the thinnest film reported here (40 nm), we observe that ~20% of the areal fraction of the surface is made up of the mixed-phase regions and that this fraction decreases steadily to zero by 300 °C, resulting in a terraced surface with unit-cell step heights corresponding to the M<sub>II</sub> phase [Figs. 4(a)–4(c)]. We note that similar stripe-like mixed-phase regions are found to reappear upon cooling, but despite similarities in the location of features, they do not appear to have an exact memory for location and fine structure. Similar decreasing trends in the fraction of the mixed phase are observed for both the 110- and 250-nm-thick films; however, both of these films still exhibit a significant fraction of mixed phases even at 300 °C (which is the maximum we can achieve in our scanning probe system). Thus, we conclude that the temperature at which the film transforms to being composed entirely of the M<sub>II</sub> phase is a function of the film thickness and is higher for thicker films. This suggests that the films form the mixed phase upon cooling down from the growth temperature, and there exists a critical thickness at which the film will stabilize in the mixed-phase structure, even at the growth temperature of 700 °C.

As illustrated by the AFM experiments, these samples exhibit a temperature-induced reduction in the fraction of the mixed phase. We note that these results are consistent with the work in the supplementary materials of Ref. 8, where phase field simulations suggest a driving force for the stabilization of the highly distorted M<sub>II</sub> phase with increasing temperature. We see that films up to a thickness of ~30 nm grow as

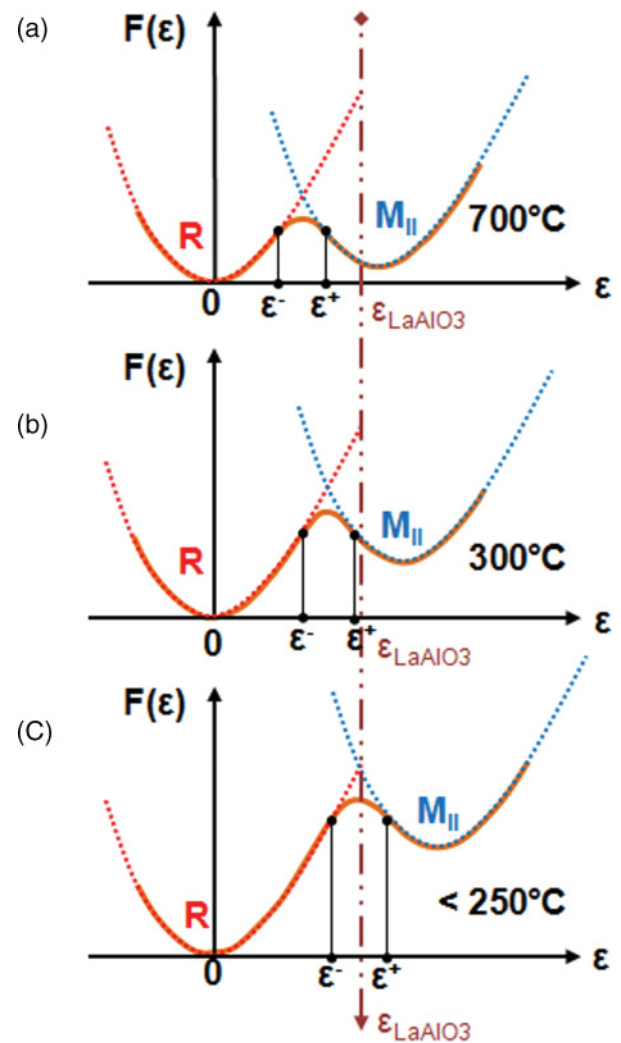


FIG. 5. (Color online) Schematic illustration of the anticipated evolution of free energy of a 40-nm-thick film as a function of thin-film strain. Upon transitioning from (a) 700 °C to (b) 300 °C to (c) <250 °C, we anticipate movement of the free-energy curves such that spontaneous formation of the mixed-phase structures occurs as noted.

the M<sub>II</sub> phase, which is stable down to room temperature. However, in thicker films (40–200 nm), we contend that the samples grow as a fully strain-stabilized, M<sub>II</sub> phase at 700 °C, and, upon cooling, the mixed-phase structures are formed to accommodate the increase in strain energy. This suggests that the formation of the mixed-phase structure stabilizes the strained film at lower temperatures. It would appear in this system that instead of generating misfit dislocations in the sample, the material undergoes partial relaxation via the formation of the M<sub>I</sub> and M<sub>II,tilt</sub> mixed-phase regions. We also note that these mixed-phase stripe bands generally form two-dimensional (2D) arrays in the film with the long axis of the bands running along [100] and [010] in-plane directions. Such a configuration has parallels to classic 2D arrays of misfit dislocations.

We can better understand the nature of the formation of such mixed-phase structures during the cool-down process by investigating the energetics of the system. Figures 5(a)–5(c) show a

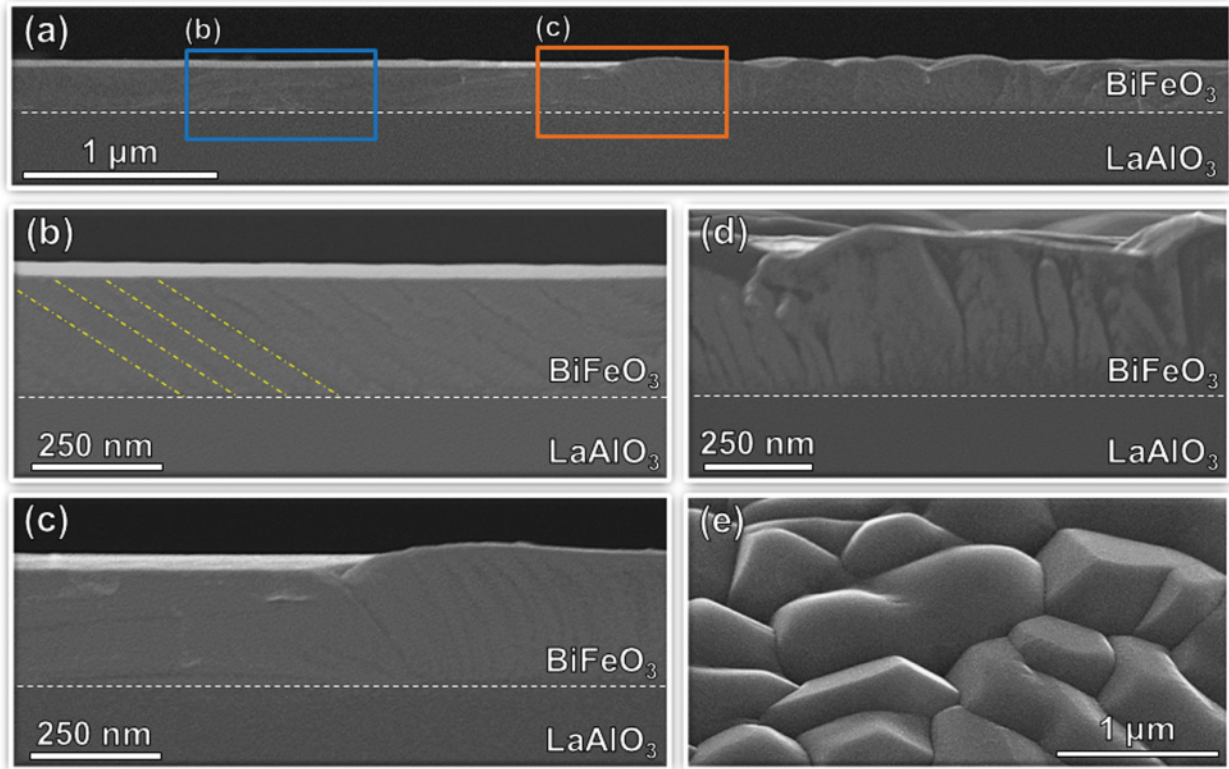


FIG. 6. (Color online) Cross-sectional SEM analysis of a 250 nm BiFeO<sub>3</sub>/LaAlO<sub>3</sub> (001) heterostructure. (a) Low-resolution view of sample shows transition from smooth to rough patches. (b) Close inspection of smooth areas reveals the presence of contrast consistent with mixed-phase region. (c) The rough, patchy regions are found to extend throughout the thickness of the film and have a fairly sharp boundary between regions. Analysis of thicker (350 nm) films reveals (d) the presence of fully epitaxial breakdown with uniform structure throughout the thickness of the film and (e) the presence of faceted crystallites on the surfaces.

schematic of the free-energy landscape for films with thickness between 40–200 nm as a function of substrate-induced strain ( $\epsilon$ ) at different temperatures. In Fig. 5, we focus on a film with a thickness of 40 nm as an example. Theoretical calculations and experimental studies have suggested the presence of a number of different structural varieties of distorted BiFeO<sub>3</sub> with a range of  $c/a$  lattice parameter ratios,<sup>13,29,30</sup> the most important of which for this discussion are the parent R phase and the highly distorted, strain-induced M<sub>II</sub> phase. Thus the energy landscape should be characterized by at least two local minima corresponding to these two phases. At the growth temperature (700 °C), we can thus draw a schematic energy diagram as a function of thin-film strain, such as that in Fig. 5(a). Consistent with previous experimental and density functional theory studies, growth at low strain levels (less than ~4% compressive strain) results in the formation of films possessing the R-phase structure, while growth at strain levels in excess of 4% results in stabilization of the M<sub>II</sub> phase. Since the R phase is the thermodynamically stable equilibrium phase at low temperature and strain, the effect of cooling the film down from the growth temperature is to shift the energy minima for the strained, metastable M<sub>II</sub> phase to higher energies and strains relative to the R phase. Thus, as we cool the film from the growth temperature down to 300 °C, the energy curves shift as noted. The region within the interval  $[\epsilon^-, \epsilon^+]$  with a negative curvature for the free energy forms a strain-induced spinodal, and in this

interval of substrate-induced strain, the film spontaneously splits to a modulated mixed-phase structure of alternating R- and M<sub>II</sub>-like phases. The region of negative curvature shifts toward the strain condition for the film on the LaAlO<sub>3</sub> substrate upon cooling from the growth temperature [Fig. 5(b)]. Between 250 and 300 °C, the fraction of mixed phase is found to become nonzero as the LaAlO<sub>3</sub> substrate forces the strain condition of the film into the strain-induced spinodal [Fig. 5(c)].<sup>18,31</sup> In this region, the film is mechanically unstable against local strain wave distortions, and this drives a lowering of the energy by spontaneous deformation to the mixed-phase structures along the easy strain axes ( $\langle 100 \rangle$ ). Therefore, films exposed to these strain conditions, as a result of the interplay between thermal expansion mismatch, epitaxial strain, and thermodynamic phase stability, will spontaneously separate into a modulated mixed-phase structure of alternating R-like and M<sub>II</sub>-like phases in the BiFeO<sub>3</sub> system.

The majority of our discussion thus far has focused on films with thicknesses of less than 200–250 nm, but beyond this critical thickness, we have observed epitaxial breakdown in these films. We now focus on the nature of this epitaxial breakdown. Figure 6(a) is a SEM cross section of a 250-nm-thick BiFeO<sub>3</sub>/LaAlO<sub>3</sub> (001) film that was observed to have a small fraction of the rough regions reported in the optical micrographs [Fig. 2(e)]. The presence of these rough regions marks the initial onset of epitaxial breakdown of the film. The SEM cross section cuts across an optically smooth

region as well as the rough region [Fig. 6(a)]. A closer look at the cross section of the optically smooth regions [blue box in Fig. 6(a), Fig. 6(b)] reveals a mixed-phase structure composed of alternating regions of  $M_I$  and  $M_{II,tilt}$  phases with sharp well-defined interfaces (emphasized by the yellow dotted lines). Focusing, in turn, on the interface between the smooth and rough regions [orange box in Fig. 6(a), Fig. 6(c)], we observe the formation of microcrystallites of the bulk R phase [consistent with AFM and x-ray diffraction studies] and that the breakdown, once initiated, is not limited to the surface but occurs through the entire thickness of the film. Note that the peak-to-valley roughness in these rough regions are found to be, in general, a good fraction of the entire film thickness, as measured via AFM. Figure 6(d) is a cross-sectional image of a 350-nm-thick film that reveals a complete breakdown of the film. Plan-view images [Fig. 6(e)] show sharp faceted microcrystallites of the R phase over the entire surface, indicating a complete breakdown of epitaxy.

Based on these results, we can now begin to construct a structural phase diagram [Fig. 7(a)] at the deposition temperature of 700 °C to help explain the evolution of the complex structure and morphology of these highly strained  $\text{BiFeO}_3$  films as a function of increasing film thickness.

An understanding of the evolution of these structures at the growth temperature is important since there are some structural evolutions that are not reversible (e.g., epitaxial breakdown), and thus the final structure of some phases will be set at the growth temperature. In the following discussion, we will also elaborate on additional structural evolution that would occur during cooling as necessary. We note that this phase diagram is similar to the diagram proposed by Bruinsma and Zangwill<sup>18</sup> for unrelated systems. The diagram shows the expected microstructure of the film as a function of epitaxial lattice mismatch between film and substrate and film thickness. Focusing first on the lattice misfit corresponding to the  $\text{LaAlO}_3$  substrate, we note that for thickness  $< 200$  nm, films grow (at 700 °C) in the pure  $M_{II}$  phase and are coherently strained to the substrate [Fig. 7(b)]. The growth is expected to occur in a layer-by-layer or step-flow growth mode as the resulting  $M_{II}$  phase regions reveal atomically flat terraces following growth. Note that films in excess of 35 nm will undergo a temperature-induced spinodal phase separation upon cooling. As the films with the strain-stabilized  $M_{II}$  phase grow in thickness, so does the cost in free energy compared to the ground-state R phase. At a critical thickness, energetics require that the films undergo a first-order transformation to the bulk, stable crystal structure.

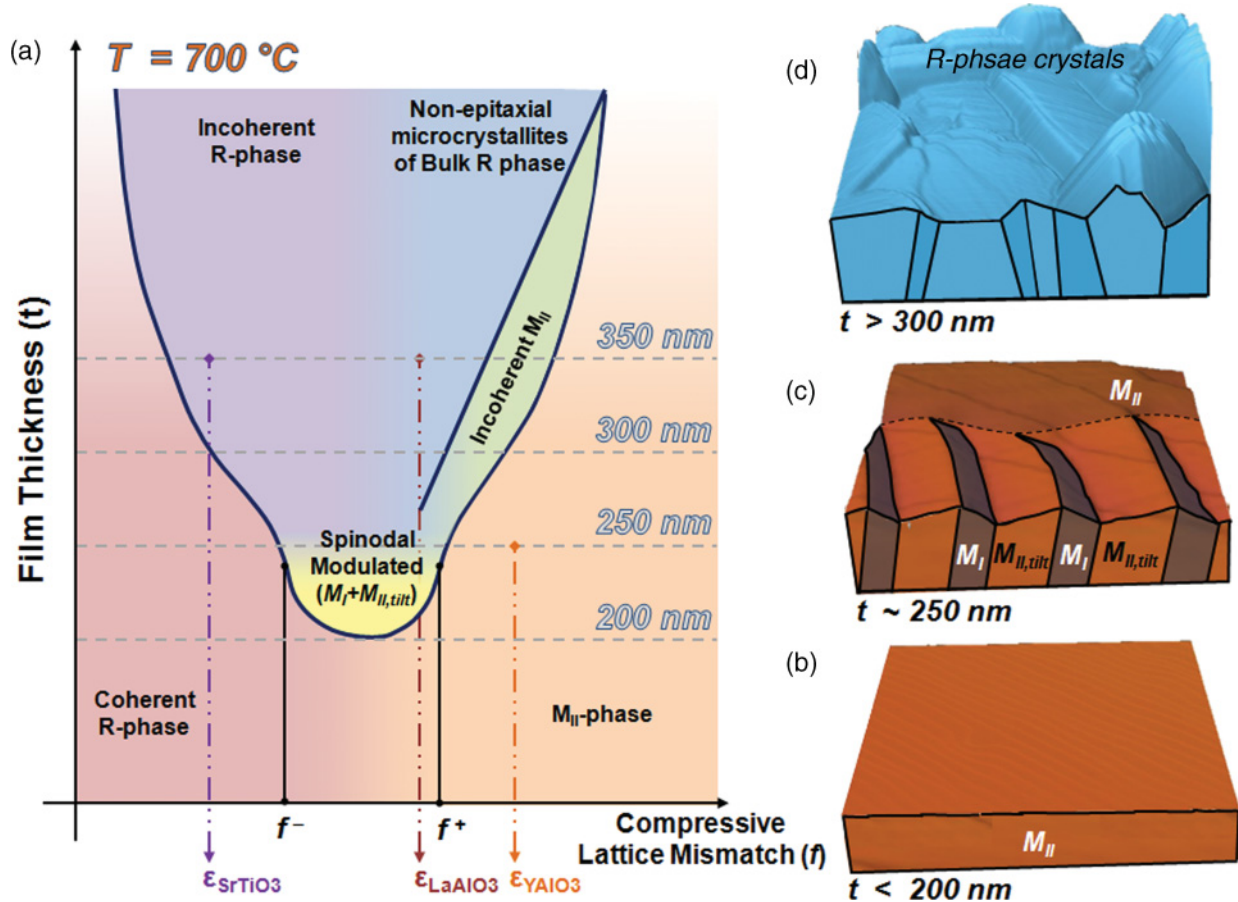


FIG. 7. (Color online) (a) Schematic phase diagram showing the evolution of the microstructure as a function of epitaxial lattice mismatch ( $f$ ) and film thickness ( $h$ ) at a growth temperature of 700 °C. At the lattice mismatch expected between  $\text{BiFeO}_3$  and  $\text{LaAlO}_3$ , we expect three different stages of growth: (b) coherent growth of the highly distorted  $M_{II}$  phase in thin films, (c) relaxation by formation of spinodal modulated structure of the  $M_I$  and  $M_{II,tilt}$  phases at intermediate thicknesses, and (d) eventual relaxation and transformation to nonepitaxial microcrystals of bulk R phase. All images correspond to structures at 700 °C.

TABLE I. Expected structural composition for BiFeO<sub>3</sub>/LaAlO<sub>3</sub> heterostructures at various temperatures and film thicknesses. Mixed phase refers to intimate mixtures of the M<sub>I</sub> and M<sub>II,tilt</sub> phases.

Film Thickness (nm)	Temperature (°C)		
	25	300	700
< 30	M <sub>II</sub>	M <sub>II</sub>	M <sub>II</sub>
40	M <sub>II</sub> + mixed phase	M <sub>II</sub>	M <sub>II</sub>
110	M <sub>II</sub> + mixed phase		M <sub>II</sub>
250	M <sub>II</sub> + mixed phase + small regions of R-microcrystallites		
350	Breakdown to R-microcrystallites		

← Mixed-phase fraction increases

However, large crystallographic deformations and geometric constraints associated with such a transformation present substantial kinetic barriers to the nucleation and transformation to the bulk, stable phase and this prevents the observation of the true equilibrium structure. As the film thickness approaches ~250 nm, it enters the regime of high-temperature, thickness-driven, strain-relaxation-induced spinodal instability and forms a strain-modulated structure of alternating M<sub>I</sub> and M<sub>II,tilt</sub> phases at the growth temperature of 700 °C [Fig. 7(c)]. The spontaneous transformation to the mixed-phase structure is accompanied by surface topography with depressions that are easily several nanometers deep (roughly 4–5% of the film thickness) and results in the significant roughening of the growth front (i.e., the sawtooth structure reported previously).<sup>9</sup> Several theoretical and experimental studies of systems undergoing spinodal phase separation and concomitant roughening of the growth front have demonstrated changes in growth mode resulting in film-to-island morphological transitions, including possible film breakup.<sup>32,33</sup> Moreover, such a mixed-phase structure with periodic interphase boundaries and surface structures significantly lowers the kinetic barriers to the nucleation of the bulk R phase and, as it approaches a thickness of 300–350 nm, the film breaks down to nonepitaxial microcrystallites of the bulk R phase [Fig. 7(d)]. Arresting growth between the 250–300 nm thickness and cooling to room temperature results in films exhibiting a mixture of the rough regions corresponding to epitaxial breakdown and mixed-phase regions, with some fraction of the flat plateaus of the M<sub>II</sub>-phase and the mixed-phase bands possessing the M<sub>I</sub> and M<sub>II,tilt</sub> phases. We summarize the expected structure at the growth temperature (700 °C), an intermediate temperature (300 °C), and room temperature (25 °C) for films of various thickness in Table I.

Furthermore, this phase diagram is consistent with previously observed work on BiFeO<sub>3</sub> thin films grown on other sub-

strates. For instance, growth of BiFeO<sub>3</sub> on YAlO<sub>3</sub> (110) substrates [ $a = 3.71$  Å, large lattice mismatch, Fig. 7(a)] has been found to result in essentially phase-pure M<sub>II</sub>-phase films up to thicknesses of 225–250 nm.<sup>8</sup> Likewise much work on BiFeO<sub>3</sub> thin films on SrTiO<sub>3</sub> (001) substrates [ $a = 3.905$  Å, small lattice mismatch, Fig. 7(a)] has been reported, and it has been observed that BiFeO<sub>3</sub> films will relax to incoherent (relaxed) films at thicknesses in excess of a few hundred nanometers.<sup>13</sup> Such results are consistent with this proposed diagram.

#### IV. CONCLUSIONS

These results have added to our understanding of these complex and technologically exciting phase boundaries in highly strained BiFeO<sub>3</sub> thin films. The presence of a variety of polymorphs of BiFeO<sub>3</sub> is essential for the strong electromechanical response observed in these films. We observe, however, that these structures are limited by a thickness-dependent breakdown and irreversible transformation to a nonepitaxial R phase. We have examined the thickness dependence and temperature dependence of these structures, and have constructed schematic energy and phase diagrams to help explain the structural evolution of these materials. We have drawn parallels to observations of unusual strain relaxation in more simplistic metallic systems, and have applied a model for spinodally modulated structures to BiFeO<sub>3</sub>. The ability of the BiFeO<sub>3</sub> system to take on a variety of polymorphs provides one route to strain relaxation and, due to the complex interplay of lattice and electronic order in these materials, this results in strong electromechanical responses. Our observations provide insights into the nature of the phase evolution in highly compressively strained BiFeO<sub>3</sub>, as well as the stability of the various polymorphs, and are consistent with previously observed structures in a variety of epitaxial BiFeO<sub>3</sub> films. Equipped with such an understanding of the thickness-driven breakdown of epitaxy, we can begin to construct pathways to stabilize the desired mixed-phase structures in these exciting and technologically relevant materials.

#### ACKNOWLEDGMENTS

The authors would like to acknowledge the help and scientific insights of Dr. M. Sardela at the Center for Microanalysis of Materials at UIUC. The work at UIUC was supported by the US Army Research Office under Grant No. W911NF-10-1-0482 and by Samsung Electronics Co., Ltd. under Grant No. 919 Samsung 2010-06795. Experiments at UIUC were carried out in part in the Frederick Seitz Materials Research Laboratory Central Facilities, which are partially supported by the US Department of Energy under Grants No. DE-FG02-07ER46453 and No. DE-FG02-07ER46471.

\*lwmartin@illinois.edu

<sup>1</sup>W. Eerenstein, N. D. Mathur, and J. F. Scott, *Nature (London)* **442**, 759 (2006).

<sup>2</sup>L. W. Martin, Y.-H. Chu, and R. Ramesh, *Mater. Sci. Eng. R* **68**, 89 (2010).

<sup>3</sup>F. Kubel and H. Schmid, *Acta Crystallogr.* **46**, 698 (1990).

<sup>4</sup>C. Ederer and N. A. Spaldin, *Phys. Rev. Lett.* **95**, 257601 (2005).

<sup>5</sup>P. Ravindran, R. Vidya, A. Kjekshus, H. Fjellvag, and O. Eriksson, *Phys. Rev. B* **74**, 224412 (2006).



- <sup>6</sup>D. Ricinchi, K.-Y. Yun, and M. Okuyama, *J. Phys. Condens. Matter* **18**, L97 (2006).
- <sup>7</sup>H. Béa, B. Dupé, S. Fusil, R. Mattana, E. Jacquet, B. Warot-Fonrose, F. Wilhelm, A. Rogalev, S. Petit, V. Cros, A. Anane, F. Petroff, K. Bouzehouane, G. Geneste, B. Dkhil, S. Lisenkov, I. Ponomareva, L. Bellaiche, M. Bibes, and A. Barthélémy, *Phys. Rev. Lett.* **102**, 217603 (2009).
- <sup>8</sup>R. J. Zeches, M. D. Rossell, J. X. Zhang, A. J. Hatt, Q. He, C.-H. Yang, A. Kumar, C. H. Wang, A. Melville, C. Adamo, G. Sheng, Y.-H. Chu, J. F. Ihlefeld, R. Erni, C. Ederer, V. Gopalan, L. Q. Chen, D. G. Schlom, N. A. Spaldin, L. W. Martin, and R. Ramesh, *Science* **326**, 977 (2009).
- <sup>9</sup>A. R. Damodaran, C.-W. Liang, Q. He, C.-Y. Peng, L. Chang, Y.-H. Chu, and L. W. Martin, *Adv. Mater.* **23**, 3170 (2011).
- <sup>10</sup>R. K. Vasudevan, Y. Liu, J. Li, W.-I. Liang, A. Kumar, S. Jesse, Y.-C. Chen, Y.-H. Chu, V. Nagarajan, and S. V. Kalinin, *Nano Lett.* **11**, 3346 (2011).
- <sup>11</sup>B. Dupé, I. C. Infante, G. Geneste, P.-E. Janolin, M. Bibes, A. Barthélémy, S. Lisenkov, L. Bellaiche, S. Ravy, and B. Dkhil, *Phys. Rev. B* **81**, 144128 (2010).
- <sup>12</sup>D. Mazumdar, V. Shelke, M. Iliev, S. Jesse, A. Kumar, S. V. Kalinin, A. P. Baddorf, and A. Gupta, *Nano Lett.* **10**, 2555 (2010).
- <sup>13</sup>H. M. Christen, J. H. Nam, H. S. Kim, A. J. Hatt, and N. A. Spaldin, *Phys. Rev. B* **83**, 144107 (2011).
- <sup>14</sup>Z. Chen, Z. Luo, C. Huang, Y. Qi, P. Yang, L. You, C. Hu, T. Wu, J. Wang, C. Gao, T. Sritharan, and L. Chen, *Adv. Funct. Mater.* **21**, 133 (2011).
- <sup>15</sup>G. W. MacDougall, H. M. Christen, W. Siemons, M. D. Biegalski, J. L. Zarestky, S. Liang, E. Dagotto, and S. E. Nagler, e-print [arXiv:1107.2975](https://arxiv.org/abs/1107.2975).
- <sup>16</sup>J. Kreisel, P. Jadhav, O. Chaix-Pluchery, M. Varela, N. Dix, F. Sanchez, and J. Fontcuberta, *J. Phys. Condens. Matter* **23**, 342202 (2011).
- <sup>17</sup>K. Y. Choi, S. H. Do, P. Lemmens, D. Wulferding, C. S. Woo, J. H. Lee, K. Chu, and C. H. Yang, *Phys. Rev. B* **84**, 132408 (2011).
- <sup>18</sup>R. Bruinsma and A. Zangwill, *J. Physique* **47**, 2055 (1986).
- <sup>19</sup>W. D. Nix, *Metall. Trans. A* **20**, 2217 (1989).
- <sup>20</sup>L. B. Freund and S. Suresh, *Thin Film Materials: Stress, Defect Formation, and Surface* (Cambridge University Press, New York, 2003).
- <sup>21</sup>Y. Kuk, L. C. Feldman, and P. J. Silverman, *Phys. Rev. Lett.* **50**, 511 (1983).
- <sup>22</sup>A. T. Fiory, J. C. Bean, L. C. Feldman, and I. K. Robinson, *J. Appl. Phys.* **56**, 1227 (1984).
- <sup>23</sup>R. F. C. Farrow, *J. Vac. Sci. Technol. B* **1**, 222 (1983).
- <sup>24</sup>R. F. C. Farrow, D. S. Robertson, G. M. Williams, A. G. Cullis, G. R. Jones, I. M. Young, and P. N. J. Dennis, *J. Cryst. Growth* **54**, 507 (1981).
- <sup>25</sup>G. A. Prinz, *Phys. Rev. Lett.* **54**, 1051 (1985).
- <sup>26</sup>D. Lebeugle, D. Colson, A. Forget, M. Viret, P. Bonville, J. F. Marucco, and S. Fusil, *Phys. Rev. B* **76**, 024116 (2007).
- <sup>27</sup>S. Lee, T. Choi, W. Ratcliff, R. Erwin, S.W. Cheong, and V. Kiryukhin, *Phys. Rev. B* **78**, 100101(R) (2008).
- <sup>28</sup>M. K. Singh, W. Prellier, M. P. Singh, R. S. Katiyar, and J. F. Scott, *Phys. Rev. B* **77**, 144403 (2008).
- <sup>29</sup>A. J. Hatt, N. A. Spaldin, and C. Ederer, *Phys. Rev. B* **81**, 054109 (2010).
- <sup>30</sup>O. Diéguez, O. E. González-Vázquez, J. C. Wojdel, and J. Íñiguez, *Phys. Rev. B* **83**, 094105 (2010).
- <sup>31</sup>P. C. Clapp, *Phys. Status Solidi B* **57**, 561 (1973).
- <sup>32</sup>A. Boyne, S. A. Dregia, and Y. Wang, *Appl. Phys. Lett.* **99**, 063111 (2011).
- <sup>33</sup>W. M. McGee, R. S. Williams, M. J. Ashwin, and T. S. Jones, *Surf. Sci.* **600**, 194 (2006).